*Bulletin of the New Zealand Society for Earthquake Engineering, Vol. 56, No. 2, June 2023*

# ASSESSMENT OF THE TORSIONAL BEHAVIOR OF HOLLOW-CORE SLABS

**Ana I. Sarkis[1], Timothy J. Sullivan[2], Emanuele Brunesi[3] and Roberto Nascimbene[4]**

(Submitted *November 2021*; Reviewed *July 2022*; Accepted *February 2023*)

**ABSTRACT**

There are many applications in buildings in which precast pre-stressed hollow-core (HC) slabs are subjected to shear, torsion, or combined shear and torsion. Nonetheless, extruded HC units contain no transverse reinforcement, being inherently vulnerable to brittle failure modes due to shear and torsional actions. In previous work by the authors, a finite element (FE) modelling approach for HC units failing in shear was developed and validated against experimental test data. This paper aims to extend the applicability of the proposed FE approach to help improve the understanding of the torsional behavior of HC units. For this purpose, the developed model is further validated against experimental data available in the literature and then used to predict the torsional capacity of New Zealand-specific 200 mm deep HC units. Results suggest that the FE model is capable of predicting the capacity of HC slabs with and without eccentricity of the applied vertical load. Finally, the numerical results are used to evaluate the performance of available simplified analysis approaches for assessing the torsional capacity of HC units, which are found to be non-conservative if used with expected material properties.

https://doi.org/10.5459/bnzsee.1572

## INTRODUCTION

Owing to the manufacturing process, extruded precast pre-stressed hollow-core (HC) units contain no transverse or vertical reinforcement in their webs. HC units contain large voids in their cross-section geometry to reduce weight, the thin-walled elements on hollow-cores will be able to include only a few coarse aggregate grains at the width of their cross-section. Furthermore, a dry concrete mix is used in the extrusion process, which is capable of meeting specific requirements such as low-slump, high early strength of the concrete, low theological strain, and small aggregate sizes. All these factors make these slabs inherently vulnerable to brittle failure modes, such as web cracking. This vulnerability is exacerbated when the slabs are subjected to shear and torsional actions [1], since, once torsional cracking develops, the torsional resistance of the hollow-core unit decreases rapidly [1-3] affecting the shear and flexural capacity of the slabs. Nonetheless, there are many applications in buildings in which HCHC slabs are subjected to shear, torsion, or combined shear and torsion.

A significant amount of research has investigated, experimentally, numerically and analytically, the shear behavior of HCHC slabs. Several researchers [4-11] evaluated the flexural and shear behavior of hollow-core slabs under the effect of different variables through experimental testing. Likewise, previous studies have provided numerical predictions of the shear behavior of HC slabs [7,8,12-15]. Frequently, the experimental or numerical results obtained were compared against the provisions found in commonly used design standards, and, in most cases, the inadequacy of analytical formulations adopted in the design of different HC slab types was underlined. Therefore, some researchers presented procedures for predicting the shear capacity taking into consideration aspects such as the hollow-core shape and depth, the related non-circularity of the voids, inherent web width variation along depth and concrete cords above and below the void [13,16,17].

Whilst the flexural and shear behavior of HC slabs has been well studied, the literature related to the behavior of HC slabs under torsional actions, or shear actions combined with torsion, is less extensive. Untopped HC units have been experimentally tested under eccentric loading to assess their behavior under pure torsion [18] and a combination of shear and torsion [19]. The experimental results were compared with available simplified analysis approaches for estimating the torsional capacity of HC units, finding inconsistencies suggesting that the simplest beam theory is too rough to properly model a single HC unit subjected to point loads very close to the support. Broo et al. [1,2] analysed the shear and torsion interaction in HC units through numerical modelling and presented the results in the form of shear-torsion interaction diagrams. The numerical models developed were able to predict the behavior of the units up to the formation of torsional cracking, but not at higher displacements. Finally, Jurkowska et al. [20] presented a technique, based on the processing of numerical data obtained using a finite element (FE) approach, for determining the flexural stiffness of hollow-core units with respect to the formation of cracks and the change in the torsional stiffness.

In New Zealand, a research programme named ReCast Floors was started in 2018 [21], aimed at expanding the current knowledge of the seismic behavior of precast concrete floors under different earthquake-induced actions. To reach this goal, experiments are being combined with FE modelling of HC units, connections and diaphragms. The research presented in this paper is part of this programme, and its main objective is to improve understanding of the torsional behavior of HC units through nonlinear FE modelling. HC units in New Zealand contain no web reinforcement, and so, their dependable performance in torsion is limited to actions that they can resist before torsional cracking occurs. Constitutive models, based

[1] *Corresponding Author, Structural Engineer, Canada, asarkisfernandez@rjc.ca*
[2] *Professor, University of Canterbury, Christchurch, timothy.sullivan@canterbury.ac.nz (Member)*
[3] *Researcher, Fondazione Eucentre, Italy, emanuele.brunesi@eucentre.it*
[4] *Associate Professor, IUSS - Scuola Universitaria Superiore Pavia, Italy, roberto.nascimbene@iusspavia.it*

on nonlinear fracture mechanics, have bene used to numerically predict the torsional capacity of HC units and to evaluate the simplified methods available of the analysis of these units under torsional actions.

In a previous phase of this research programme, a three-dimensional numerical modelling approach, and critical modelling criteria, for HC units failing in shear, were proposed [15]. This paper tests the applicability of the proposed FE approach to HC units subjected to torsional actions. For this purpose, this study uses experimental test data available in the literature [18,19] to validate the FE modelling approach for the failure mechanisms attributed to torsion or, more in general, to a combination of shear and torsion.

The validated model will then be used to numerically predict the torsional capacity of New Zealand 200 mm deep HC units. This slab depth is the most commonly used precast flooring element in New Zealand [22], and hence is the focus of this research. Finally, the results obtained are compared against simplified analysis approaches available in New Zealand [3,23,24], which are based on the method proposed by Mitchell & Collins [25] and Collins & Mitchell [26].

## TORSIONAL BEHAVIOR OF PPHC UNITS

### Torsional Actions Induced in PPHC Units

A significant amount of research has been done on shear in HC units. Torsion has not been seen as a problem for hollow-core floors in buildings when these have been designed as simply-supported one-way span elements subjected to gravity loading only, unless high concentrated loads are applied. This is due to the floor having a high torsional stiffness in the direction along the precast units and low flexural stiffness in the transverse direction, which gives a predominant one-way action. However, when the HC units are subjected to earthquake actions, problems may arise if the units are supported in a non-uniform way. Differential rotations of the supporting structure at each end of the unit may induce twisting about its longitudinal axis (see Figure 1a). This can be particularly critical when combined with seismic loading, where the supports will deform differently as the building sways laterally. On the other hand, no differential support movement inducing torsion on the HC units would be expected in a symmetric regular building.

There are many building applications where torsional cracking of HC slabs may be induced due to differential deflection of the supporting structure. For example, potential problems may arise in buildings with moment resisting frames with no corner columns [3], where one end of a unit is supported on a beam, which remains relatively straight as the building sways in an earthquake, while the other end is supported by a cantilever beam (see Figure 1b). Similar situations arise when a HC slab is supported on one end on a coupling beam between two walls, on the active link of an eccentrically braced frame. In both cases, the other end of the slab is assumed to be supported by framing that does not rotate to the same extent as inter-story drift occurs. Further examples of cases when significant twisting of the units might occur are described by Mostafa et al. [27].

In all the cases described, significant twists are applied to the hollow-core units, which can be expected to cause extensive diagonal cracking. In these situations, while the torsional strength is not important, Fenwick et al. [3] argue that it is essential to limit the twist so that the flexural and shear capacities of the hollow-core are not degraded by diagonal cracking associated with torsion.

### Estimation of the Torsional Capacity

HC units under torsional actions are commonly assumed to act in a manner that mimics a box section, and their performance is usually assessed by codified criteria up to the load stage where torsional cracking occurs. The existing expressions to estimate the torsional cracking capacity, found in Collins & Mitchell [28] and adopted in the New Zealand guidelines and standards [3,23,24], are briefly reviewed herein.

Torsion in HC units is predominantly resisted by a shear flow in the outside webs, the soffit of the slab and the concrete topping (see Figure 2a). The torsional loading causes shear stresses acting mainly in the perimetric zone of the cross-section. In the outermost webs and in the flanges, these stresses act together with the normal stresses, $f_{pc}$, introduced by the pre-stressing. The actual stress combination and the thickness of the flanges and the outermost webs, $t$, determine whether the cracking starts in a web or in one of the flanges. The shear stress, $v$, caused by the applied torsional moment $T$, is given by Eq. (1) [28]:

$$v = \frac{T}{2A_o t} \tag{1}$$

where $A_o$ can be calculated by transforming the cross-section of the hollow-core unit into an equivalent tubular cross-section (see Figure 2b), as per Eq. (2):

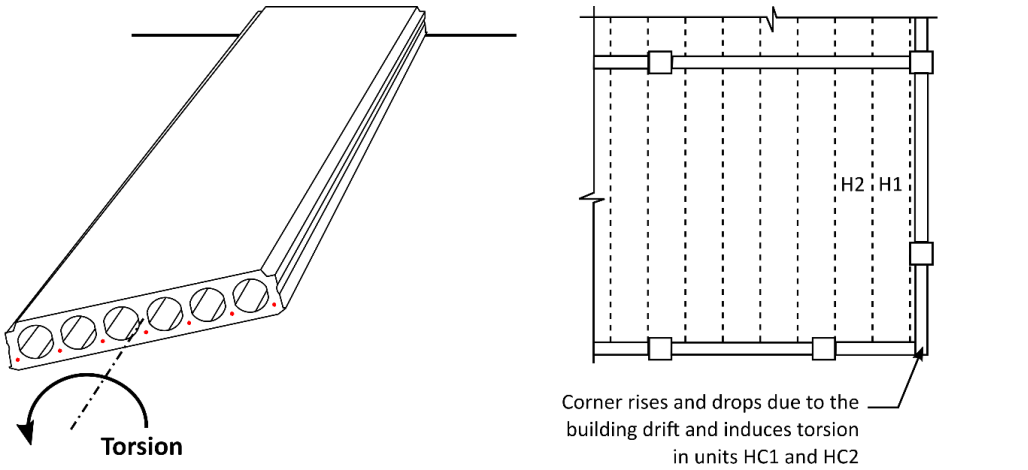


(a) Torsional actions imposed due to differential deflection of supporting structure

(b) Example of units vulnerable to induced torsion (plan view of frame building without corner columns

***Figure 1: Torsional actions induced in hollow-core slabs (modified from [3]).***

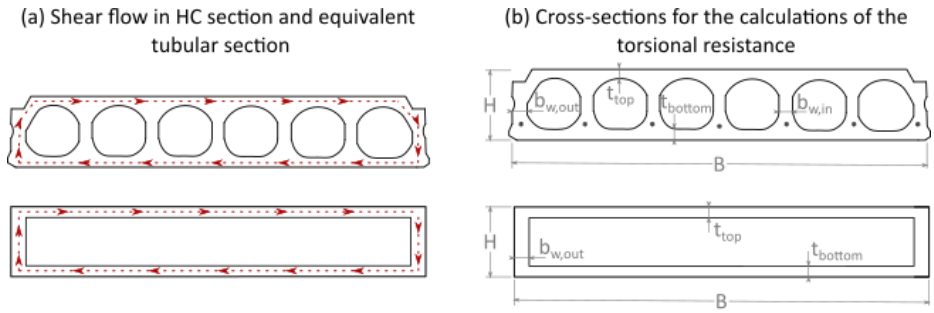


***Figure 2: Equivalent tube for assessing torsional cracking.***

$$A_o = \left[H - \frac{(t_{top} + t_{bottom})}{2}\right](B - b_{w,out}) \quad (2)$$

where, $B$ is the width of the section, $b_{w,out}$ is the outer webs thickness, and $t_{top}$ and $t_{bottom}$ are the top and bottom flange thicknesses, respectively. In Eq. (1), $t = t_{top}$ in calculations for the top flange, whereas $t = b_{w,out}$ in those for the outermost webs. However, the thickness, $t$, may not be larger than $t_c$, the latter being expressed according to Eq. (3) [28]:

$$t_c = \frac{3}{4}\frac{A_c}{p_c} \quad (3)$$

where $A_c$ is the total area enclosed by the total outside perimeter of the concrete cross-section, and $p_c$ is the outer circumference of the transformed cross section. While the area enclosed by the shear flow path, $A_o$, could be calculated from the external dimensions and wall thicknesses of the equivalent tube, it is a reasonable approximation to take $A_o$ as 2/3 of $A_c$ [28]. Hence, from Eq. (1) and Eq. (3), $\nu$ can be calculated as reported in Eq. (4):

$$\nu = \frac{T p_c}{A_c^2} \quad (4)$$

Diagonal torsional cracks will occur when the principal tensile stress reaches the cracking strength of the concrete $f_{ct}$. Then, the stress that will cause torsional cracking can be expressed as in Eq. (5):

$$\nu = f_{ct}\sqrt{1 + \frac{f_{pc}}{f_{ct}}} \quad (5)$$

Combining this expression with Eq. (4), the cracking torsional moment, $T_{cr}$, of a pre-stressed concrete member is given by Eq. (6) [28]:

$$T_{cr} = \frac{A_c^2}{p_c} f_{ct}\sqrt{1 + \frac{f_{pc}}{f_{ct}}} \quad (6)$$

The stiffness of the slab can be estimated by equating the internal strain energy and the work done by the external forces. The energy from the external forces is equal to $^1/_2\, T_{cr}\theta_{cr}$, where $\theta_{cr}$ is the angle of twist over the length of slab being considered [29]. The internal energy, $\varepsilon_{int}$, is equal to the strain energy associated with the shear deformation around the section. Therefore, $\theta_{cr}$ is given by Eq. (7):

$$\theta_{cr} = 2\frac{\varepsilon_{int}}{T_{cr}} \quad (7)$$

Finally, the limiting twist to prevent diagonal cracks from eliminating the flexural strength, $\theta_{fl}$, is taken as follows (see Eq. (8)):

$$\theta_{fl} = \frac{2.5}{\emptyset_{df}}\theta_{cr} \quad (8)$$

where $\emptyset_{df}$ is the deformation factor, and can be taken as 1.25 [29]. Fenwick et al. [3] recommend using this factor where deformations are critical in assessing a collapse mechanism. This factor allows for the inherent scatter in deformation predictions and can be used either to increase the predicted deformation in assessment or to reduce the maximum permitted design deformation or in this case twist. Further description of this simplified assessment approach for HC units can be found in Mostafa et al. [27].

**Experimental Testing of PPHC Slabs**

Past testing data has been re-examined to bring together an experimental database of six simply supported single 200 mm deep HC units subjected to torsional and shear-torsional actions. Two 200 mm deep HC units tested under solely torsional actions [18], and four shear-torsion interaction tests [19] were selected. The testing procedure and results are summarized herein, which will later be used to inform the FE approach discussed later in this paper.

***Table 1: Concrete and pre-stress properties of the HC units tested by Pajari [18,19].***

| Concrete section | | Pre-stressing steel | |
|---|---|---|---|
| Cross sectional area (mm$^2$) | 1.22 x 10$^5$ | Number of strands | 7 |
| Second moment of area (mm$^2$) | 6.13x10$^8$ | Strands diameter (mm) | 12.5 |
| Compressive strength (MPa) | 60 | Area of pre-stressing steel (mm$^2$) | 651 |
| Modulus of rupture (MPa) | 4.13 | Ultimate tensile strength (MPa) | 1860 |
| Modulus of elasticity (GPa) | 33 | Initial pre-stress (MPa) | 900 |
| | | Transfer length strands (mm) | 625 |

Table 1 presents the concrete and pre-stress properties of the HC units tested, further dimensions of the cross-section of the units is later shown in Figure 11. Figure 3 schematically shows the pure torsion test set-up used for the two units tested under torsional actions alone [18]. The active end of the slab is free to rotate around the axis parallel to the longitudinal axis of the slab (y-axis). At the passive support, the slab can move

longitudinally along the y-axis. The HC slab was loaded by two equal point loads P at opposite sides of the centreline of the slab. To stabilize the specimen, the load at the passive end had a slightly greater eccentricity than that at the active end (see Figure 3). The tests were carried out under displacement control, and the elongation of the actuator at the active end was used to control the applied displacements at both supports. The test specimens were instrumented with eight transducers to measure the vertical displacement of the slab at both supports, which allowed the angle of twist of the slab to be estimated.

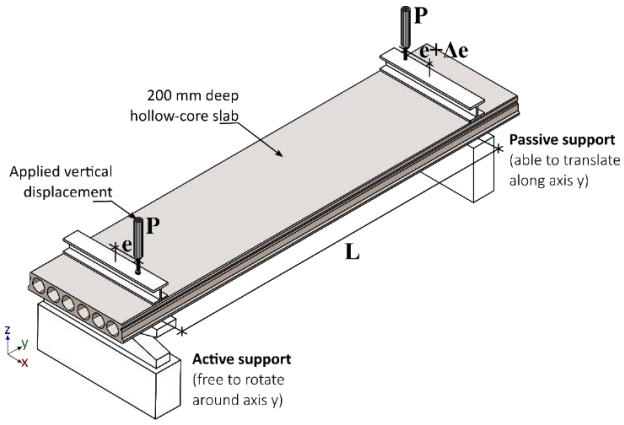


***Figure 3: Experimental set-up used on the pure torsion tests of hollow-core units* [18].**

Table 2 provides some characteristics of the pure torsion test specimens, PT200A and PT200B, as well as measured resistance against torque and angle of twist before cracking. Both specimens are 5000 mm long, with a separation between supports of 4000 mm.

Figure 4 presents the support conditions and loading arrangements for the four shear-torsion interaction tests considered in this study [19]. Just as in the pure torsion tests, in the shear-torsion interaction tests the loaded end of the slab is called the active support, and the opposite end is the passive support. There were two-point loads on the webs of the slab unit. The loading was either centric or eccentric with respect to the longitudinal centreline of the slab. In every case, the load P was applied at a distance $a$ from the active support equal to 2.5 times the depth of the unit. All specimens had a total length of 7060 mm and a distance between supports of 7000 mm. The deflection was measured by transducers placed vertically on the corners of the slab and at both supports.

The failure load for each specimen is presented in Table 3, as well as the load corresponding to the first observed crack. The failure load is taken as the making load before an abrupt and severe drop in torsional resistance (torsional strength capacity) took place. As shown in Figure 4b, specimen ST200C had concentric loading and no torsional actions.

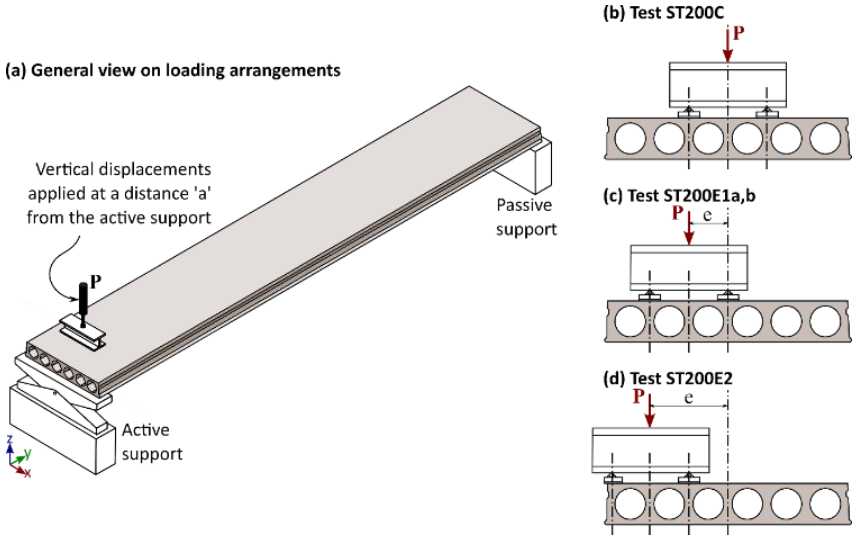


***Figure 4: Experimental set-up used for the shear-torsion interaction testing of hollow-core units [19].***

***Table 2: Summary of pure torsion tests used for the FE model calibration [18].***

| Test specimen | Thickness | Total length | Span length | Eccentricity | Resistance against torque | Angle of twist before cracking |
|---|---|---|---|---|---|---|
| | **H** (mm) | $\mathbf{L_T}$ (mm) | **L** (mm) | **e** (mm) | $\mathbf{T_{exp}}$ (kNm) | $\boldsymbol{\varphi_{exp}}$ (mrad) |
| PT200A | 200 | 5000 | 4000 | 300 | 37.5 | 4.86 |
| PT200B | 200 | 5000 | 4000 | 300 | 39.4 | 5.35 |

***Table 3: Summary of shear-torsion interaction tests used for the FE model calibration [19].***

| Test specimen | Thickness | Total length | Span length | Eccentricity | Resistance against torque | Angle of twist before cracking |
|---|---|---|---|---|---|---|
| | **H** (mm) | $\mathbf{L_T}$ (mm) | **L** (mm) | **e** (mm) | $\mathbf{T_{exp}}$ (kNm) | $\boldsymbol{\varphi_{exp}}$ (mrad) |
| PT200A | 200 | 5000 | 4000 | 300 | 37.5 | 4.86 |
| PT200B | 200 | 5000 | 4000 | 300 | 39.4 | 5.35 |

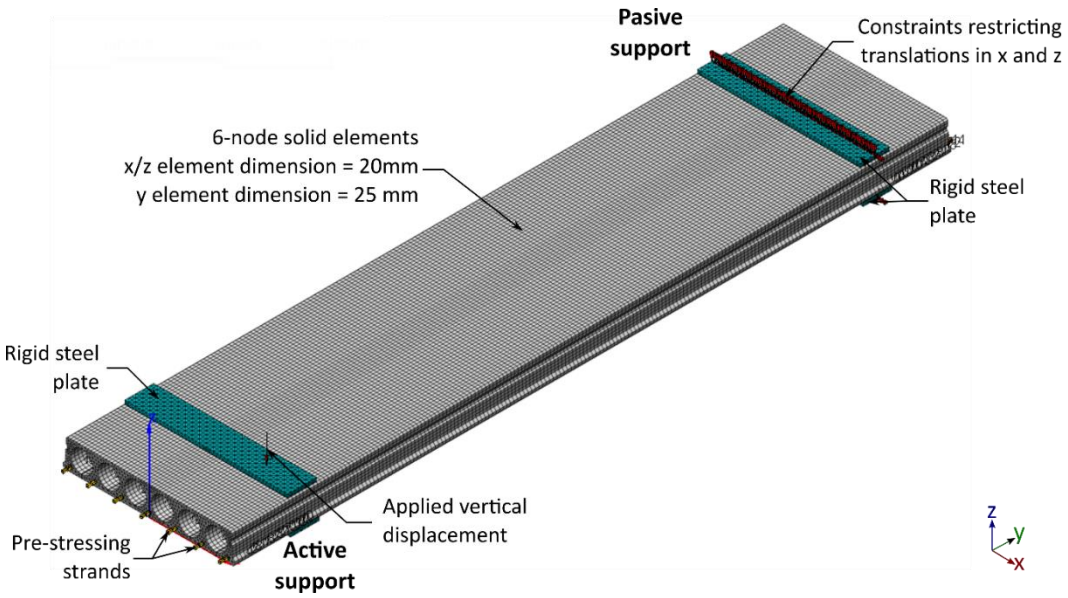


***Figure 5: Example of detailed solid finite element models developed.***

## FINITE ELEMENT MODELLING APPROACH

### Proposed Numerical Approach

To investigate the behavior of HC units, three-dimensional FE models have been created using the software Midas FEA [30], which allows consideration of both mechanical and geometrical non-linearity. This FE modelling approach had been first developed by the authors to study HC units failing in shear [15], and calibrated against full-scale three-point bending tests [11]. The research presented herein investigates what extensions of the FE approach are required for the cases of pure torsion and shear-torsion interaction on HC units.

Figure 5 shows the detailed three-dimensional mesh for the solid FE model of the 200 mm deep units under pure torsion. The concrete has been modelled using 6-node brick elements. The constitutive model assumed for the concrete is the smeared total strain crack model. This model is based on the modified compression field theory, originally proposed by Vecchio & Collins [31], and then extended to the three-dimensional case by Selby & Vecchio [32]. Moreover, a rotating cracking constitutive model was selected, in which the directions of the cracks are assumed to continuously rotate depending on the changes in the axis of the principal strains [31]. The constitutive model was assumed to adopt the Hordijk model [33,34] and the Thorenfeldt model [35] for uniaxial tensile and compressive behavior, respectively.

The mean compressive strength $f_c$, and the modulus of rupture $f_r$, of the hollow-core extruded concrete have been obtained through material characterisation testing carried out by the authors [11]. The fracture energy $G_f$ and the crack bandwidth $h$, required to define the tensile behavior or the concrete, have been deterministically estimated as follows [36,37]:

$$G_f = 73 f_c^{0.18} \quad (9)$$

$$h = 2.1 d_{agg} \quad (10)$$

where, $d_{agg}$ is the maximum aggregate size in mm.

The pre-stressing strands are represented in the model as embedded line elements. The stress in the pre-stressing strands can be represented as an equivalent parabolic pre-stress distribution, according to the work presented by Yang [17], where the strand stress is postulated to be zero at the free ends of the slabs and to achieve the full effective stress at the end of the transfer length of the strands. Therefore, no interface elements were introduced to represent strands-concrete interaction, since it is implicitly captured by an equivalent parabolic pre-stress distribution [17]. The classical Von Mises yielding criterion with strain hardening was used for the pre-stressed steel strands. Final pre-stressing, after losses, as well as the corresponding transfer length to be used in the finite element model can be calculated according to NZS3101:2006-A3 [23].

Rigid steel plates with the same dimensions as those used during the experimental testing have been modelled at the top and bottom of the unit at both supports. The main role of the passive support is to prevent rotation and translation along the longitudinal axis, and so, a transversal row of constraints has been placed at the passive support, where the rigid steel plates had been placed, to restrict the translations in the x and z directions (see Figure 5). At the active support, a pinned constraint was placed in the bottom rigid plate, at the centreline of the slab, to allow rotations around the y-axis. For the pure torsion case, displacement has been imposed at a point on the top plate of the active support at distance $e = 300$ mm from the slab's centreline. For the shear-torsion interaction case, displacements have been applied at two points at a distance $a$ = 500 mm from the active support with an eccentricity as defined in Table 3 and shown in Figure 4b-d. Even though the support conditions were simplified during the modelling, the numerical results obtained indicated that the supports behavior was close to the experimental observations, and no significant differences were observed in the initial stiffness of the units.

### Finite Element Model Validation

In this section, the accuracy of the FE predictions obtained for the six specimens analysed is quantified via comparison with the experimental data. For this purpose, the obtained loads and displacements at failure, the crack pattern, and the cross-section deformation from both tests and analyses are presented.

*Pure Torsion*

Table 4 presents a comparison between the experimentally observed and numerically predicted torsional moment and twisting capacity of the specimens tested in pure torsion. Similarly, Figure 6 illustrates the torque versus rotation

relationship observed for specimens PT200A and PT200B. In the experiments, slabs PT200A and PT200B showed a resistance against torque of 37.5 and 39.4 kNm respectively, with an average torsional moment capacity of 38.4 kNm. The FE model predicted a maximum torsional moment of 38.8 kNm, which differs by 3% and 2% respectively from the experimental torsional moment $T_{exp}$ observed for specimens PT200A and PT200B, as shown in Table 4.

In the case of the angle of twist at failure, the difference was more substantial as the numerical model predicted an angle of 6.08 mrad, whereas during the experiments an angle of 4.86 and 5.35 mrad was observed, leading to an overestimation of the angle of twist of 22 and 13%, respectively. Furthermore, in Figure 6 it can be observed that the FE model provided a reasonable approximation of the torsional stiffness and response of the HC slabs.

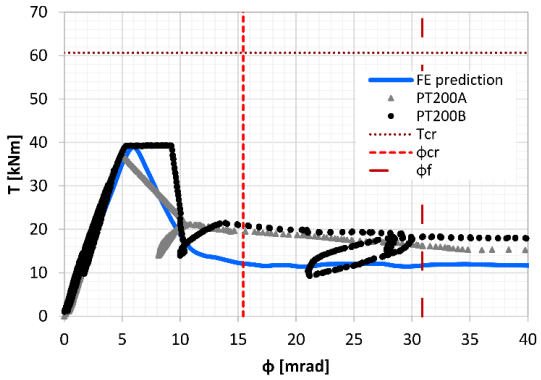


***Figure 6: Comparison of the experimental and numerical torque and relative angle twist relation.***

Figure 7 shows the numerically predicted principal tensile stress distribution after failure, overlapped with the cracking traced from the experimental testing for specimens PT200A and PT200B. In both the tests and the FE simulation, the first cracks appeared transversally at the top of the slab close to the passive support, as was expected from a theoretical point of view. The specimen's failure was brittle and therefore the first cracks coincide with the peak torsional moment, which is followed by an abrupt and permanent reduction in torque. In both experiments and modelling results, a similar post-peak behavior can be observed in the moment-twist behavior. After the abrupt drop in torque, due to the formation of the transverse cracks, the torsional moment stayed at a relatively constant residual value with increasing applied rotation. This has been observed previously in the shear-displacement response of HC units [11]. This apparent residual capacity, present after a brittle failure took place, can be attributed to factors such as surface friction, the dowel action of the longitudinal reinforcement and the bond between strands and concrete due to mechanical interlock. Large uncertainty is associated with the extend of the contribution of each of these factors to the measured residual capacity of the slabs.

For the experimental results, the post-cracking torsional resistance is roughly 50% of the maximum torque resistance, whereas the post cracking torsional resistance obtained numerically is about 35% of the maximum torque resistance. This shows that the model adequately predicted the post cracking mechanism and underpredicts the post-cracking residual moment capacity of the units. The comparison of the experimental and numerical results shows that the proposed FE modelling approach is able to adequately capture the damage progression of the PPHC slabs, and the post-cracking nonlinear mechanism at higher or even much higher displacements. The model provided a satisfactory prediction of the elastic torsional stiffness of the units and the maximum torsional moment capacity, however, it overestimated the associated angle of twist at which the torsional cracking occurred and underestimated the post-peak moment capacity. The differences in the angle of twist range between 0.73 and 1.22 mrad. Considering this and low deformability of the HC slabs, it is hard to determine how much of this difference comes from the model uncertainty and how much comes from different sources of error while testing. In addition, future experimental research efforts should further investigate the factors affecting the post-peak regime that contribute to the residual moment capacity of the units.

***Table 4: Comparison of experimental results and FE predictions for the pure torsion tests.***

| Test specimen | Resistance against torque | | | Angle of twist before cracking | | |
|---|---|---|---|---|---|---|
| | Exp. value $T_{exp}$ (kNm) | FE prediction $T_{FE}$ (kNm) | Prediction/ Experiment | Exp. value $\varphi_{exp}$ (mrad) | FE prediction $\varphi_{FE}$ (mrad) | Prediction/ Experiment |
| PT200A | 37.5 | 38.8 | 1.03 | 4.86 | 6.08 | 1.22 |
| PT200B | 39.4 | 38.8 | 0.98 | 5.35 | 6.08 | 1.13 |

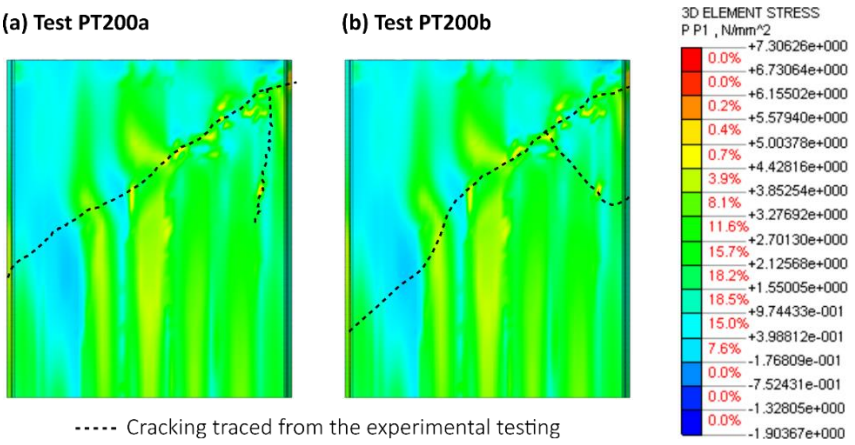


***Figure 7: Comparison of the principal tensile stresses against the experimentally observed cracking after failure.***

*Table 5: Comparison of experimental results and finite element predictions for the shear-torsion interactions tests.*

| Test specimen | Eccentricity **e** (mm) | Failure Load $F_{max,exp}$ (kN) | FE prediction $F_{max,FE}$ (kN) | Prediction/Experiment |
|---|---|---|---|---|
| ST200C | 0 | 135.6 | 129.5 | 0.95 |
| ST200E1a | 187 | 100.4 | 106.4 | 1.06 |
| ST200E1b | 187 | 98.4 | 106.4 | 1.08 |
| ST200E2 | 384 | 64.4 | 68.5 | 1.06 |

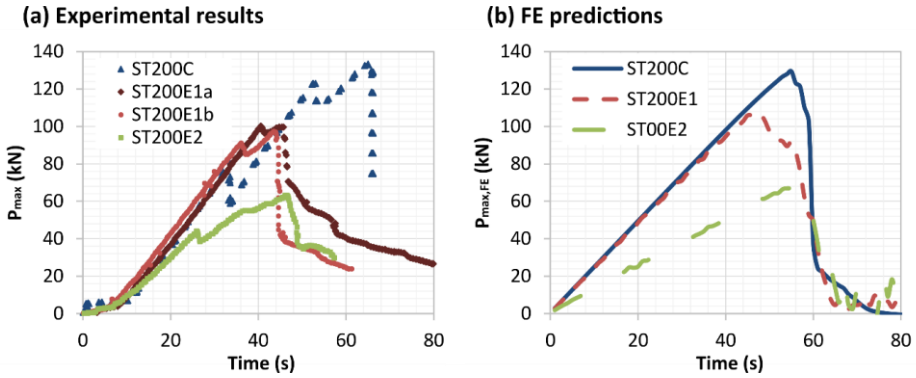


*Figure 8: Comparison of the experimental and numerical loading for the shear-torsion interaction tests.*

*Shear-Torsion Interaction*

Torsion on a HC unit generates shear stresses acting upwards in one of the outermost webs and downwards in the other. In the case of vertical shear forces, shear stresses will be ideally uniformly distributed over all webs. Therefore, when shear and torsion act simultaneously on a HC unit, these stresses will sum, meaning that one of the outermost webs will receive much higher stresses than the rest of the webs. The FE force predictions for the shear-torsion interaction tests are summarized in Table 5 and compared against the experimental results. The progression of the load over the loading time for both tests, as per Pajari (2004b), and FE predictions are shown in Figure 8a and Figure 8b, respectively.

The peak load predicted for specimen ST200C is 129.5 kN, which differs by 5% with the experimental peak force of 135.6 kN. As this specimen had no eccentric loading, these results can be used as a baseline to determine the influence of the force eccentricity on the behavior of the other specimens. The observed failure, in both model and experiment, was brittle due to web shear cracking.

The load was applied with an eccentricity E1 = 187 mm for specimens ST200E1a and ST200E1b, as shown in Figure 4c. The maximum load reached by these specimens, experimentally, is 100.4 and 98.4 kN, respectively. As shown in Table 5, the FE prediction for the specimens with an eccentricity E1=187 mm is 106.4 kNm, these values are 6% and 8% larger than the peak load obtained experimentally for specimens ST200E1a and ST200E1b, respectively. For specimen ST200E2, the load was imposed with a larger eccentricity E2 = 384 mm (see Figure 4d). The specimen failed at an experimental maximum load of 64.4 kN. Here again, the maximum force predicted for specimen ST200E2 is 68.5 kN, which is 6% larger than the maximum force obtained for the same specimen experimentally. Furthermore, in Figure 8 it can be observed that the FE model provided a good approximation of the stiffness of the HC units in all cases. The comparison between the experimental results and the FE prediction for the shear-torsion interaction tests show that the proposed FE approach is able to predict the capacity of the HC units with or without eccentrically applied loads.

From the experimental results, it should be noted that the specimen with the larger torsional action (ST200E2), due to a bigger eccentricity E2, failed at a load that was 52% smaller than the specimen with no torsional actions (ST200C). Similarly, the specimens with the 187 mm eccentricity E1 failed at an average load 27% smaller than the specimen with no torsional actions, confirming the influence that torsional cracking has in the shear capacity of simply supported HC units. The same can be observed from the FE predictions, where the maximum load predicted for specimen ST200E2 is 48% smaller than the load predicted for specimen ST200C, and 36% smaller than the load predicted for specimens ST200E1a and ST200E1b. Therefore, it is confirmed that the model is also capable of predicting the influence that torsional cracking has on the shear capacity of the HC units.

During the testing of specimen ST200C, at peak load, the three central webs of the slab developed diagonal web-cracks, while the other webs remained intact (Figure 9a). In the model, the central web cracked first, as shown in the principal tensile stress distribution in Figure 9b. This event was followed by the cracking of the other internal webs, with the two outermost webs remaining intact. In both cases, the failure was brittle, with a complete drop in the resistance once the peak force is reached.

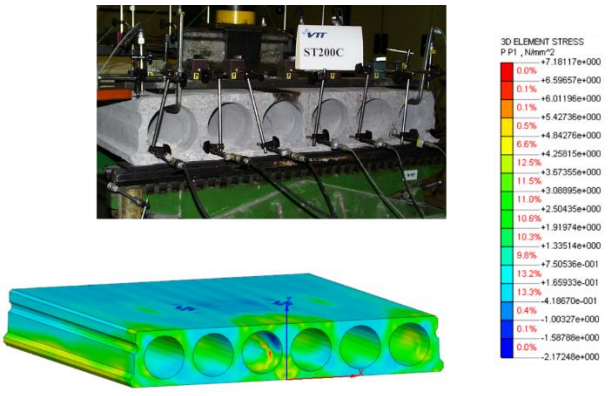


*Figure 9: Comparison of the principal tensile stresses for specimen ST200C with the experimental observations.*

All specimens eccentrically loaded, and tested in a combination of shear and torsion, exhibited brittle failures due to diagonal web cracking. Good consistency between the experimental and numerical crack patterns was observed in all cases. To illustrate the comparison of results, Figure 10 shows the principal tensile stresses at failure obtained for the specimen with eccentricity E1 and compares it against the cracking traced from the experimental observations for specimen ST200E1a. During the test, at peak load, the two outermost webs on the side of the applied load failed in web shear, as well as the central web. Similar behavior was observed in the numerical prediction in Figure 10 where cracking has taken place in the outermost and central webs, on the side of the applied load. Additionally, there is congruence between the experimental and numerical cracking observed at the top of the hollow-core unit, where cracks were observed at the top of the outermost void and the two central voids (Figure 10).

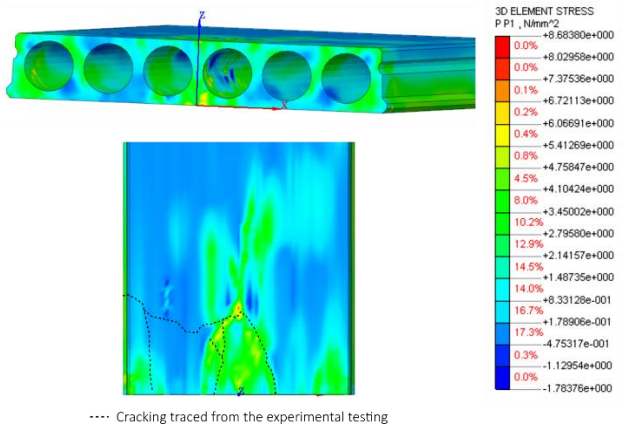


***Figure 10: Principal tensile stresses for specimen ST200E1 and comparison against the experimental cracking traced from ST200E1a.***

## EVALUATING THE PERFORMANCE OF SIMPLIFIED ANALYSIS METHODS

The proposed FE modelling approach, validated against experimental data, was used to model a 200 mm deep unit that is typical in New Zealand, specimen PT200NZ, to numerically assess its torsional moment and twist capacity. The properties of the concrete and pre-stressing steel are outlined in Table 6 below, and cross-sectional dimensions are shown in Figure 11. Further details about the characteristic of this New Zealand-specific units can be found in Sarkis et al. [11].

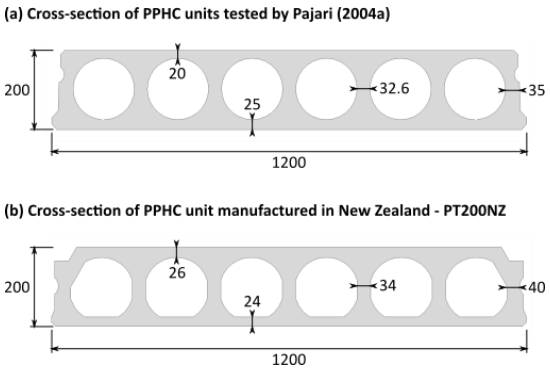


***Figure 11: Cross section geometry of the HC units: (a) tested by Pajari [18]; and (b) manufactured in New Zealand. All measurements are in mm.***

Additionally, the moment and twist capacity of the HC units has been estimated following the design and assessment provisions found in New Zealand [23,24,29], which in turn refer to the method proposed by Collins & Mitchell [28], which was outlined earlier in this paper.

***Table 6: Concrete and pre-stress properties of the typical New Zealand HC unit modelled.***

| **Concrete section** | | **Pre-stressing steel** | |
|---|---|---|---|
| Cross sectional area ($mm^2$) | 1.21 x $10^5$ | Number of strands | 7 |
| Unit weight (kg/m) | 386 | Strands diameter (mm) | 12.7 |
| Second moment of area ($mm^2$) | 6.57x$10^8$ | Area of pre-stressing steel ($mm^2$) | 690 |
| Compressive strength (MPa) | 80 | Ultimate tensile strength (MPa) | 1860 |
| Modulus of rupture (MPa) | 6.5 | Modulus of Elasticity (GPa) | 195 |
| Tensile fracture energy (N/mm) | 0.16 | Pre-stress losses | 12% |
| Crack bandwidth (mm) | 25 | Transfer length strands (mm) | 635 |

Table 7 summarizes the results obtained through the FE prediction of the New Zealand-specific unit. The FE model did not differ from the model developed in the validation in its boundary conditions and loading. The HC slab reached a maximum moment of 60.3 kNm at an applied twist of 9.5 mrad. The overall torsional behavior was similar to that observed for specimens PT200A and PT200B. The relationship between the applied twist and the resulting torsional moment is shown in Figure 12. It can be observed that the torsional moment *T* increases linearly until the first crack appears, which is followed by an immediate and sudden drop in the torque capacity. Past the peak moment, the nonlinear behavior of the HC slab is characterized by a relatively constant residual capacity as the twist increases.

***Table 7: Comparison of the FE-predicted torsional capacity with the simplified analysis method presented in Section 2.***

| | **Torsional cracking moment** | | **Torsional cracking rotation** | |
|---|---|---|---|---|
| **FE prediction** | $T_{FE}$ (kNm) | 60.3 | $\varphi_{FE}$ (mrad) | 9.8 |
| **Theoretical estimation 1*** | $T_{t,1}$ (kNm) | 72.2 | $\varphi_{t,1}$ (mrad) | 21.4 |
| | $T_{FE}/T_{t,1}$ | 0.8 | $\varphi_{FE}/\varphi_{t,1}$ | 0.5 |
| **Theoretical estimation 2**** | $T_{t,2}$ (kNm) | 29.6 | $\varphi_{t,2}$ (mrad) | 8.8 |
| | $T_{FE}/T_{t,2}$ | 2.0 | $\varphi_{FE}/\varphi_{t,2}$ | 1.1 |

** Estimated using concrete properties obtained from material testing carried out by Sarkis et al [11] and summarized in Table 6*
*** Assuming the nominal compressive strength defined by the manufacturer of 45MPa and a tensile strength of 0.33√fc*

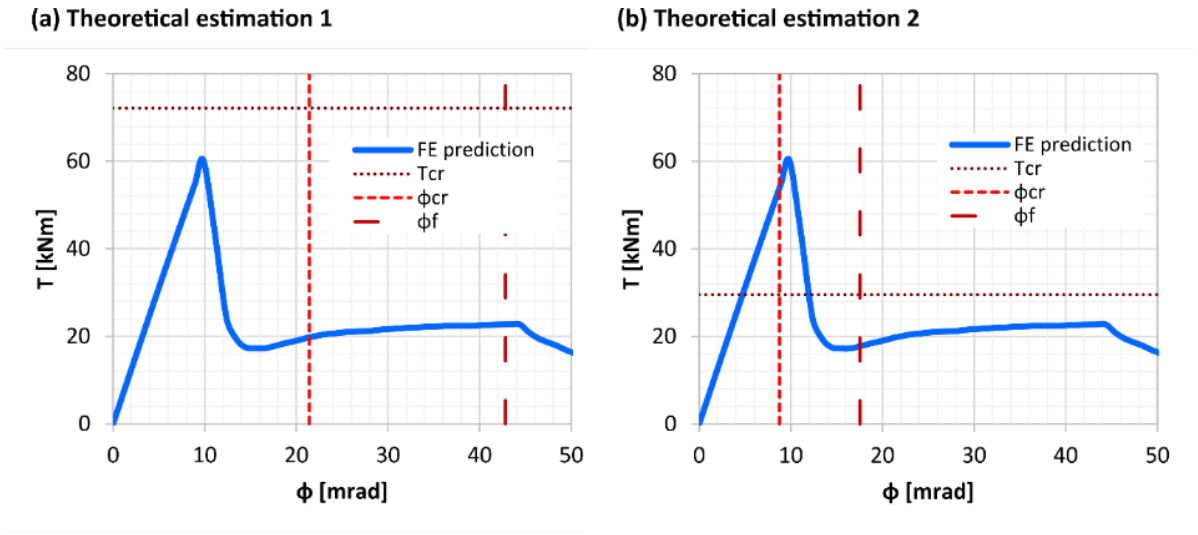


***Figure 12: Torsional capacity versus applied twist for specimen PT200NZ.***

Specimen PT200NZ exhibited greater torsional capacity than the units tested by Pajari [18]; the torque capacity obtained is 43% higher and the twist capacity 47% higher for specimen PT200NZ. For all specimens, the length of the unit, the supports and the loading arrangement were the same, with the only differences being the concrete properties and the geometry of the cross-section. The results from the material testing [11,18] show that specimen PT200NZ has a 20% higher compressive strength and a 44% higher modulus of rupture than specimens PT200A and PT200B. In addition to the concrete properties, the different geometries may be influencing the torsional behavior of the specimens studied. Figure 11 shows the cross-section for both specimens. It can be observed that specimens PT200A and PT200B have circular voids and in general thinner webs and flanges than specimen PT200NZ. In contrast, specimen PT200NZ has a more regular web width and thicker webs with non-fully circular voids. In the past, Brunesi & Nascimbene [13] analysed HC units with both circular and non-circular voids and revealed the sensitivity of the web-shear failure mechanism, and related shear capacity, to the cross-section shape, non-circularity of the voids, inherent web width variation along the unit's depth, and number of concrete chords above and below the void. Similar studies have not been done on the influence of the hollow-core cross-section geometry on the torsional behavior of the units, thus motivating further the comparison provided herein.

Torsional capacity of the HC units is estimated through the simplified analysis approach for two cases: (1) assuming the concrete properties are those obtained from the material testing [11]; and, (2) assuming the nominal compressive strength of the concrete specified by the product guidelines, provided by the hollow-core manufacturer, and a tensile strength $f_{ct} = 0.33\sqrt{f_c}$, as suggested by Collins & Mitchell [28] and Fenwick et al. [3]. For Case (1) the properties reported in Table 5 have been used, which correspond to a compressive strength of 80 MPa and a modulus of rupture of 6.5 MPa, further details about how these properties where defined can be found in Sarkis et al. [11,15]. In contrast, for Case (2) a nominal compressive strength of 45 MPa has been assumed.

The first theoretical estimation predicted a torsional moment capacity of 72.2 kNm and a twist capacity of 21.4 mrad (Table 7). These values exceeded by 20% and 50%, respectively, the finite element model prediction (see Table 7 and Figure 12a), despite the fact that this estimation made use of the same properties as the FE model. In the same way, the capacity of specimens PT200A and PT200B, tested by Pajari [18], has been estimated through the first case, using the material properties obtained from material testing and employed in the FE model. Again, the simplified analysis approach over-predicted the capacity of the HC slabs when compared to the FE and experimental results (see Figure 6). This suggests that the current guidelines in New Zealand will be non-conservative if used with expected material properties.

For the second theoretical estimation, it has been assumed that no material testing data was available, and, therefore, nominal properties of the concrete are used. As shown in Table 7 and Figure 12b, the predicted torque capacity is 29.6 kNm and the twist capacity 8.8 mrad. When compared to the FE prediction, the second theoretical estimation provided conservative values that are 50% and 10% less than the numerical predictions. These results highlight the sensitivity of the simplified analysis approach to the properties of the concrete. This is particularly relevant in the case of the HC units as it is known that the properties of the extruded concrete used during the manufacturing can greatly differ from those of the normal concrete. The results also suggest that even though the simplified approach is inaccurate, and the use of nominal material properties may be inadequate because materials are likely to be stronger than specified, the resulting error may not be huge.

HC slabs are commonly designed as simply supported elements, mainly to resist bending moments due to gravity loads. The computational analysis of such a design is normally based on the assumption of the plane stress state. Assuming a plane stress state in the cross-section of the slab is justified when the element is subjected to uniformly distributed loads over its entire surface and when it is supported on two parallel and relatively rigid supports [20,38]. Nonetheless, the response of HC units under torsional actions is much more complex as the cross-section deformations are three-dimensional, presenting secondary bending mechanisms at a cross-sectional level. Figure 13 illustrates the cross-section deformation and principal tensile stress distribution for specimen PT200NZ right before failure and at the moment of torsional failure. It can be seen that the cross-section, rather than remaining plane, deforms in the y-z plane as the member rotates around the y-axis. Furthermore, the simplified method employed for the calculations assumes a uniform flow of shear stresses $v$ around the perimeter of the cross-section, whereas the stresses presented in Figure 13 show high concentrations of tensile stresses in the top-right and bottom-left corners, and low tensile stresses in the opposing corners of the cross-section. The non-uniform deformation within the section shown in Figure 13 help explain why the simplified approach may not be conservative when used with expected properties.

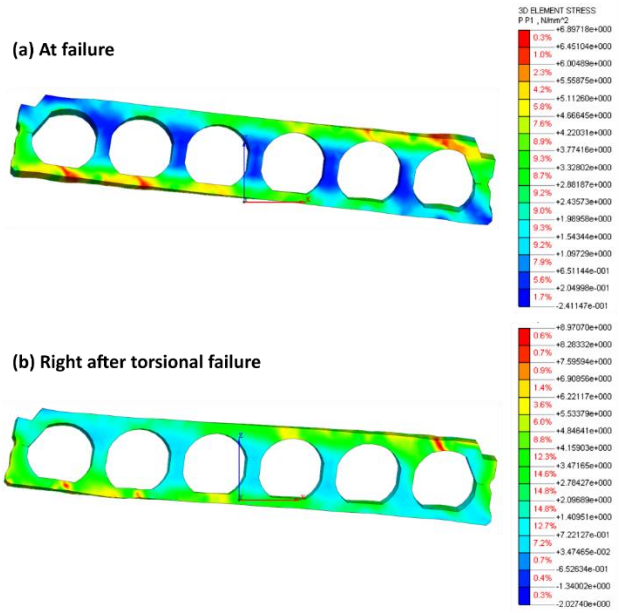


***Figure 13: Principal tensile stresses and cross-section deformations for specimen PT200NZ.***

The simplified method proposed by Collins & Mitchell [28] is based on the analysis and testing of individual members. Hence, it provides little information regarding the interaction of the member under study with other surrounding structural members. However, in a floor system, a HC unit will interact with the adjacent members, which could restrain the rotation and elongation of each individual unit and significantly affect the torsional resistance of the individual slabs. Further research is needed to quantify and comprehend the influence of this group effect on the assessment of the torsional capacity of HC slabs and mitigate torsional failures in practice.

## CONCLUSIONS

This paper has tested the applicability of a previously proposed FE approach to the modelling of HC units failing in torsion and a combination of shear and torsion, by comparing predictions with observations from experimental testing data available in the literature. In addition, the model was used to predict the torsional capacity of New Zealand-specific HC units, and the results were used to evaluate the performance of the available simplified analysis method.

The following observations and conclusions were drawn from this study:

- The proposed FE modelling approach was able to adequately capture the damage progression of bare HC units under torsional actions, as well as the post-cracking nonlinear behavior of at higher displacement demands.
- The model provided a satisfactory prediction of the elastic torsional stiffness of the units and the maximum torsional moment capacity, however, it overestimated the associated angle of twist at which the torsional cracking occurred and underestimated the post-peak moment capacity.
- The influence that torsional cracking has on the shear capacity of simply supported HC units was well captured in the numerical predictions. And so, the FE model of Sarkis et al. [15] can be used to predict the shear capacity of HC units with and without eccentricity.
- The simplified analysis method available in New Zealand Standards for assessing the torsional capacity of HC units proved to be non-conservative if expected material properties are used, in particular, the tensile strength of the concrete.
- The numerical observations showed that the cross-sectional deformations in HC units under torsion are three-dimensional and that the flow of shear stresses around the perimeter of the cross-section is non-uniform, which is conflicting with the plane stress state assumption commonly used in simplified analysis methods. This helps explain why the simplified assessment approach currently used in New Zealand is not accurate.

The research presented in this paper provides a good base for the analysis of bare HC units under torsional actions. This offers a base for future research which should study the effect of supporting elements at each end of the units with different stiffness values that are representative of real building connection detailing and supporting conditions. The results presented are limited to the analysis of individual hollow-core units. Future research efforts should look into the redistribution of loads to the adjacent precast members, and the impact of the group effect on the torsional capacity of the HC floors.

## ACKNOWLEDGEMENTS

The authors would like to acknowledge the in-kind support provided by CSP FEA for the Midas FEA software. This research is being partly funded through the BRANZ-funded ReCast Project via the University of Auckland, and their support is gratefully acknowledged. In addition, this project was partially supported by QuakeCoRE, a New Zealand Tertiary Education Commission-funded Centre. This is QuakeCoRE publication number XXXX.

## REFERENCES

1 Broo H, Lundgren K and Engström B (2005). "Shear and torsion interaction in prestressed hollow core units". *Magazine of Concrete Research*, **57**(9): 521-533. https://doi.org/10.1680/macr.2005.57.9.521

2 Broo H, Lundgren K and Engström B (2007). "Shear and torsion in prestressed hollow core units: Finite element analyses of full-scale tests". *Structural Concrete*, **8**(2): 87–100. https://doi.org/10.1680/stco.2007.8.2.87

3 Fenwick R, Bull D and Gardiner D (2010). "*Assessment of Hollow-Core Floors for Seismic Performance*". Report 2010-02. Department of Civil and Natural Resources Engineering, University of Canterbury, Christchurch, NZ.

4 Araújo D de L, Sales MWR, Silva RPM, Antunes C de FM and Ferreira M de A (2020). "Shear strength of prestressed 160 mm deep hollow core slabs". *Engineering Structures*, **218***:* 110723. https://doi.org/10.1016/j.engstruct.2020.110723

5 El-Sayed AK, Al-Negheimish AI and Alhozaimy AM (2019). "Web shear resistance of prestressed precast deep hollow core slabs". *ACI Structural Journal*, **116**(1): 139-150. https://doi.org/10.14359/51706919

6 Hawkins NM and Ghosh SK (2006). "Shear strength of hollow-core slabs". *PCI Journal*, **51**(1): 110-115.

7 Michelini E, Bernardi P, Cerioni R and Belletti B (2020). "Experimental and numerical assessment of flexural and shear behavior of precast prestressed deep hollow-core slabs". *International Journal of Concrete Structures and Materials*, **14**(1). https://doi.org/10.1186/s40069-020-00407-y

8 Nguyen TNH, Tan KH and Kanda T (2019). "Investigations on web-shear behavior of deep precast, prestressed concrete hollow core slabs". *Engineering Structures*, **183**: 579–593. https://doi.org/10.1016/j.engstruct.2018.12.052

9 Pajari M (2005). "*Resistance of Prestressed Hollow-Core Slabs Against Web Shear Failure*". VTT Technical Research Centre of Finland. https://www.vtt.fi/inf/pdf/tiedotteet/2005/T2292.pdf

10 Palmer KD and Schultz AE (2011). "Experimental investigation of the web-shear strength of deep hollow-core units". *PCI Journal*, **56**(4): 83–104. https://doi.org/10.15554/pcij.09012011.83.104

11 Sarkis AI, Bueker F, Sullivan TJ, Elwood KJ, Brunesi E and Hogan L (2022a). "Aspects affecting the nonlinear behavior of precast pre-stressed hollow-core units failing in shear". *Structural Concrete*, **23**(5): 3021-3038. https://doi.org/10.1002/suco.202100579

12 Brunesi E, Bolognini D and Nascimbene R (2015). "Evaluation of the shear capacity of precast-prestressed hollow core slabs: numerical and experimental comparisons". *Materials and Structures*, **48**(5): 1503–1521. https://doi.org/10.1617/s11527-014-0250-6

13 Brunesi E and Nascimbene R (2015). "Numerical web-shear strength assessment of precast prestressed hollow core slab units". *Engineering Structures*, **102**: 13–30. https://doi.org/10.1016/j.engstruct.2015.08.013

14 Pachalla SKS and Prakash SS (2018). "Load resistance and failure modes of hollow-core slabs with openings: A finite element analysis". *PCI Journal*, **63**(4): 25-40. https://doi.org/10.15554/pcij63.4-03

15 Sarkis AI, Sullivan TJ, Brunesi E and Nascimbene R (2022b). "Critical modelling criteria for precast pre-stressed hollow-core slabs". *Journal of Building Engineering*, **54**: 104545. https://doi.org/10.1016/j.jobe.2022.104545

16 Pisanty A (1992). "The shear strength of extruded hollow-core slabs". *Materials and Structures*, **25**(4): 224–230. https://doi.org/10.1007/BF02473067

17 Yang L (1994). "Design of prestressed hollow core slabs with reference to web shear failure". *Journal of Structural Engineering*, **120**(9): 2675–2696. https://doi.org/10.1061/(ASCE)0733-9445(1994)120:9(2675)

18 Pajari M (2004a). "*Pure Torsion Tests on Single Hollow Core Slabs*". VTT Research Notes 2273, 29p. ISBN: 951-38-6517-7. VTT Technical Research Centre of Finland.

19 Pajari M (2004b). "*Shear-Torsion Interaction Tests on Single Hollow Core Slabs*". Technical Report, 204pp, ISBN 951-38-6519-3. VTT Technical Research Centre of Finland. https://publications.vtt.fi/pdf/tiedotteet/2004/T2275.pdf

20 Jurkowska N, Derkowski W and Azizov T (2019). "Consideration of the torsional stiffness in hollow-core slabs' design". *Materials Science Forum*, **968**: 330–341. https://doi.org/10.4028/www.scientific.net/MSF.968.330

21 Brooke N, Elwood K, Bull D, Liu A, Henry R, Sullivan T, Hogan L and del Rey Castillo E (2019). "ReCast floors - Seismic assessment and improvement of existing precast concrete floors". *SESOC Journal*, **32**(1).

22 Puranam A, Filippova O, Pastor-Paz J, Stephens M, Elwood KJ, Ismail N, Noy I and Opabola E (2019). "A detailed inventory of medium-to high-rise buildings in Wellington's central business district". *Bulletin of the New Zealand Society for Earthquake Engineering*, **52**(4): 172–192. https://doi.org/10.5459/BNZSEE.52.4.172-192

23 SNZ (2006). "*NZS3101: Concrete Structures Standard, Part 1: The Design of Concrete Structures*". Standards New Zealand, Wellington, NZ.

24 SESOC (2017). "*The Seismic Assessment of Existing Buildings: Technical Guidelines for Engineering Assessments*". Structural engineering Society (SESOC) and Ministry of Business, Innovation, and Employment (MBIE), Wellington, NZ.

25 Mitchell D and Collins MP (1978). "Influence of prestressing on torsional response of concrete beams". *PCI Journal*, **23**(3): 54–73. https://doi.org/10.15554/pcij.05011978.54.73

26 Collins MP and Mitchell D (1980). "Shear and torsion design of prestressed and non-prestressed concrete beams". *PCI Journal*, **25**(5): 32–100. https://doi.org/10.15554/pcij.09011980.32.100

27 Mostafa M, Hogan L and Elwood KJ (2022). "Torsional capacity assessment of precast hollow-core floors". *SESOC Journal*, **35**(1): 109-124.

28 Collins MP and Mitchell D (1997). *Prestressed Concrete Structures*. Response Publications.

29 Fenwick R, Deam B and Bull D (2004). "Failure modes for hollowcore flooring units". *SESOC Journal*, **17**(1): 52–70.

30 MIDAS Information Technology (2016). *Midas FEA: Advanced Nonlinear and Detail Analysis System* (v1.1). https://www.cspfea.net/prodotti/midas-fea-nx/

31 Vecchio FJ and Collins MP (1986). "The modified compression-field theory for reinforced concrete elements subjected to shear'. *ACI Journal*, **83**(2): 219–231. https://doi.org/10.14359/10416

32 Selby RG and Vecchio FJ (1993). "*3D Constitutive Relations for Reinforced Concrete*". Technical Report 93-02, Department of Civil Engineering, University of Toronto, Canada.

33 Hordijk DA (1992). "Tensile and tensile fatigue behaviour of concrete; experiments, modelling and analyses". *Heron*, **37**(1): 1–79.

34 Reinhardt HW, Cornelissen HAW and Hordijk DA (1986). "Tensile tests and failure analysis of concrete". *Journal of Structural Engineering*, **112**(11): 2462–2477. https://doi.org/10.1061/(ASCE)0733-9445(1986)112:11(2462)

35 Thorenfeldt E (1987). "Mechanical properties of high-strength concrete and applications in design". *Proceedings of the Utilization of High-Strength Concrete Symposium*, Norway.

36 Federation Internationale du Beton (2013). "*FIB Model Code for Concrete Structures 2010*". International Federation for Structural Concrete, ISBN: 9783433030615. https://doi.org/10.1002/9783433604090

37 Malvar LJ and Fourney ME (1990). "A three dimensional application of the smeared crack approach". *Engineering Fracture Mechanics*, **35**(1–3): 251–260. https://doi.org/10.1016/0013-7944(90)90203-S

38 Derkowski W and Surma M (2015). "Torsion of precast hollow core slabs". *Technical Transactions Civil Engineering*, 13pp. https://doi.org/10.4467/2353737XCT.15.160.4335